Aberystwyth University

Simulating the Hele-Shaw flow in the presence of various obstacles and moving particles
Peck, D.; Rogosin, Sergei; Wrobel, Michal; Mishuris, Gennady

Simulating the Hele-Shaw flow in the presence of various obstacles and moving particles

D. Peck · S.V. Rogosin · M. Wrobel ·
G. Mishuris

Abstract A generalization of the approach developed in the recent papers by the authors (Mishuris *et al*) [1,2] is presented. It aims to provide a description of the Hele-Shaw cell in the presence of multiple small obstacles/moving particles. We perform an asymptotic analysis of the dynamics of the moving boundary and the moving particles. For this, a modification of Maz'ya-Movchan-Nieves uniform asymptotic formula [3] for the Green's function of the mixed boundary value problem for the Laplace equation in a multiply connected domain is utilized. The paper contains extensive numerical analysis, accounting for various physical mechanisms of particle movement in the Hele-Shaw flow.

1 Introduction

We consider a slow viscous flow in a narrow space between two parallel plates in presence of various fixed or moving obstacles. The model is a modification of the well-known Hele-Shaw moving boundary value problem [4], [5] which in turn is an analogous to a one-phase Stefan problem [6] and is a special case of the Navier–Stokes problem (see, e.g., [5]).

It is supposed that the driving mechanism for the flow is a one-point source/sink. The movement of particles in the flow depends not only on the

D. Peck · M. Wrobel · G. Mishuris
Department of Mathematics, Aberystwyth University, Penglais, SY23 3BZ, UK
E-mail: dip9@aber.ac.uk, miw15@aber.ac.uk, ggm@aber.ac.uk

S.V. Rogosin
Belarusian State University, Nezavisimosti Ave., 4, 220030 Minsk, Belarus E-mail: rogosin@bsu.by

source/sink intensity, but also on the friction between obstacles and plates, as well as on the particle interaction.

The considered problem is motivated by applications encountered in industrial settings. Foremost is the often noted example of injection moulding, where a high viscosity fluid is pumped through a strategically placed hole into a mould of prescribed shape. During the injection process air must be allowed to escape from the mould, and as such vents must be properly placed around the mould at the locations which will be the last to be filled by the fluid. In the simple case this reduces to studying the free moving boundary of a Hele-Shaw cell containing stationary obstacles (see [7] for a more extensive description).

Meanwhile the field of microfluidics presents a more recent domain in which the modeling of multiple moving inclusions within the Hele-Shaw cell may prove useful. An interesting example was given in [8], where a Hele-Shaw cell with fine patterns etched into the channel roof was utilized to control the movement of water drops within a fluid flow. Such a system has potential benefits when performing parallel experiments in molecular and cell biology, where using two-dimensional arrays enables the investigator to, in effect, obtain simplified data sets for multiple experiments simultaneously.

Additionally, the method utilized in this paper to represent inelastic collisions means that the model may be used to examine problems where particles coalesce (or 'clump'), such as the study of biological systems where agglutination occurs.

Finally it is the hope of the authors that this model may later assist in the developing of a numerical tool capable of simulating the mass transport mechanism for the fluid flow in a narrow channel. This type of problem is most notably encountered in hydraulic fracturing technologies, with respect to the slurry flow inside the fracture (see, e.g., [9], [10] and references therein).

Following [11] we reduce our problem to a mixed boundary value problem for the Laplace equation in a multiply connected domain. Supposing existence of moving particles in the flow we have to add extra equations describing this movement (also accounting for the different friction properties of the particles). Its geometric solution (parametrization of the moving front and trajectories of the moving particles) is sought from equations given in terms of the Green's function for the above mixed boundary value problem. Our main theoretical tool is an asymptotic analysis of the model based on the approximation of the Green's function.

The properties of Green's functions for various differential operators subject to different boundary conditions are of great importance in finding the solution to the above problems, and thus for many applications (see, e.g. [12], [13]). There are only a few known results for the exact representation of Green's functions which correspond to the simplest boundary conditions and simple geometry (see, e.g. [14], [15]). Therefore, elaborating on novel asymptotic and approximate methods becomes crucial to the theory and application of Green's functions. The use of asymptotic methods for approximation of Green's functions goes back to the classical paper by J. Hadamard [16], where the method of regular perturbation was performed. Recently, V. Maz'ya, A. Movchan and

M. Nieves developed the methods of asymptotic approximation and obtained several uniform asymptotic formulas for Green's functions related to different boundary value problems for a number of differential operators in the case of singular perturbations of the domains. In [17] a number of uniform asymptotic approximations of the Green's function for mixed and Neumann problems in domains with small holes/inclusions were obtained. A review of Maz'ya-Movchan-Nieves results on asymptotic expansion of the Green's function for elliptic problems in perforated domains is presented in [18]. Special attention is paid to Green's kernel for multiply connected domains in $\mathbb{R}^3$. For domains in $\mathbb{R}^2$ with several small inclusions a uniform asymptotic formula for the Green's function in transmission problems of antiplane shear was given in [19]. An extended exposition of methods and results for asymptotic approximation of Green's functions is presented in [3]. We use these results in the study of the Hele-Shaw problem in domains with several small inclusions.

This article presents an essential extension of the method proposed in [1] (for a single fixed obstacle in the Hele-Shaw flow) and in [2] (where an individual particle is supposed to move in the flow). Our first aim here is to show that the developed method continues to obtain comparably good results for several (fixed or immobile) inclusions. We note that the density, size and shape of the obstacles do not constrain our asymptotic analysis (though the computations in this paper are only dealing with circular objects; this choice has the advantage of allowing us to present the discovered features in a more straightforward manner). The more novel challenge is for us to take into account the various interactions (elastic, fully non-elastic and intermediate) between particles. We perform numerical simulations involving different scenarios of the obstacles' behavior, as well as conducting simulations with differing numbers of inclusions (up to 540).

Our paper is organized as follows. The problem formulation is given in Sec. 2, with the final set of equations relative to our model collected under the title **Problem HS$_\mathrm{M}$.**

A modification of the Maz'ya-Movchan-Nieves formula for the Green's function of a mixed boundary value problem for the Laplace equation is presented in Sec. 3. It accounts for the geometrical and physical assumptions of the considered model. The components of the proposed uniform asymptotic formula (3) are additionally presented in this chapter, while further discussion of their nature and possible representations is relegated to the supplementary material.

The final system of equations is presented in Subsec. 4.1, and a computational model is developed to solve the approximate system in Subsec. 4.2.

In Sec. 5 the accuracy of the computational model is examined, followed by the providing of numerical simulations involving different scenarios for the obstacles' movement, examining the effect of particle inclusion on the fluid flow.

We conclude in Sec. 6 with the discussion of the obtained results highlighting the different features of the flow in presence of moving obstacles.

2 Problem formulation

We consider a two-dimensional potential flow of viscous incompressible fluid in the Hele-Shaw cell caused by a source/sink placed at the origin 0 with finite number of rigid obstacles in the flow, which is supposed to be very slow. Each obstacle is moving without rotation due to the pressure in the flow. Their movement can be faster or slower depending on specific friction between an obstacle and the plates of the Hele-Shaw cell.

Let us denote by $\Omega(t) \ni 0$ an open simply connected domain encircled by the free boundary $\Gamma(t) = \partial\Omega(t)$ at each time instant $t \geq 0$. We study the flow at (in principle unknown) time interval $I = [0, T]$ which could be rather small in the case of the sink (extraction of the fluid).

The obstacles are represented by fixed shape closed subdomains of $\Omega(t)$. To avoid technical difficulties, we accept a circular shape of the the obstacles of the radius ε_k and denote the (moving) center of obstacles by $\mathbf{z}_k(t)$, i.e. $F_k(t) := \left\{ \mathbf{z} \in \mathbb{R}^2 : |\mathbf{z} - \mathbf{z}_k(t)| \leq \varepsilon_k \right\}, k = 1, \ldots, M$. The domain occupied by the fluid is denoted $\Omega_M(t) = \Omega(t) \setminus \bigcup\limits_{k=1}^{M} F_k$.
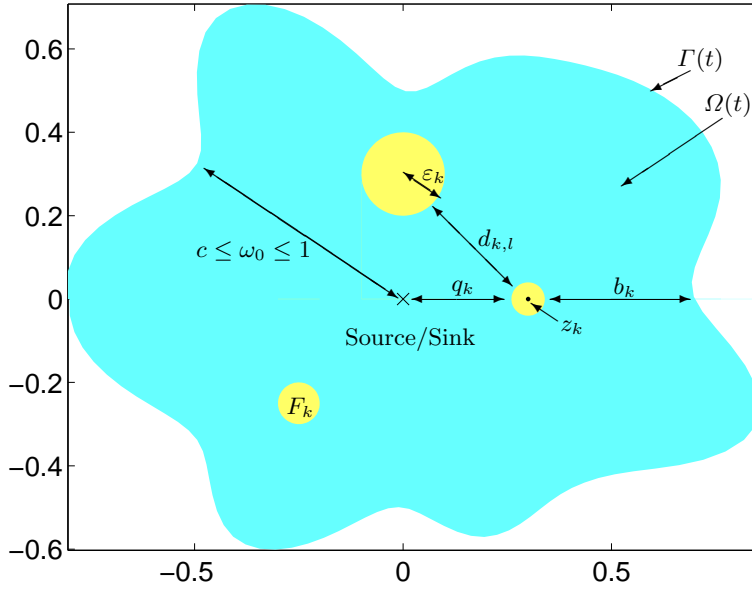

Fig. 1 Diagram of the initial configuration of the Hele-Shaw cell for an arbitrary domain Ω. Here $\omega_0 = dist\{\mathbf{0}, \Gamma(0)\}$.

This formulation is demonstrated graphically in Fig. 1, as well as certain natural assumptions which the parameters of the initial geometry must satisfy[1]:

1. **Particle distribution:**
   - The initial distribution of the particles/obstacles must not place them too close to the boundary, with the minimum distance determined by the radius of the particle. Stated explicitly: $dist\{\delta F_k(0), \delta\Omega(0)\} = b_k > \varepsilon_k$.
   - Similarly the obstacles/particles must not come too close to the source/sink, with the radius of the particle determining the minimum: $dist\{\delta F_k(0), \mathbf{0}\} = q_k > \varepsilon_k$.
   - The inclusions must not overlap with each other, this can be stated as $\bigcap_{k=1}^{M} F_k = \emptyset$. More explicitly we have, for all $k, l = 1, \ldots, M, k \neq l, t \in I$:
     $$: d_{k,l} = |z_k(t) - z_l(t)| > \varepsilon_k + \varepsilon_l$$
2. **Domain size:** The characteristic size of the initial domain $\Omega(0)$ is of order 10^0, with bounds on the minimum and maximum initial distance as follows: $0 < c \leq \min dist\{0, \Omega(0)\} \leq \max dist\{0, \Omega(0)\} \leq 1$, where $c < b_k + 2\varepsilon_k$.

In furthering the analysis, it is convenient to re-scale the domains F_k by introducing new variables

$$\xi_k = \frac{1}{\varepsilon_k}\left(\mathbf{x} - \mathbf{z}_k\right),$$

i.e. to consider the following domains

$$F_0(t) := B\left(O; 1\right). \tag{1}$$

From maximum regularity assertion for the free boundary in the Hele-Shaw problem (see [20]) it follows that initial boundary has to satisfy the condition

$$\partial\Omega(0) \in \mathcal{C}^{2,\alpha},\ 0 < \alpha < 1. \tag{2}$$

Now we are at the position to formulate our problem (cf. [5], [11]) which is a generalization of the models considred in [1], [2].

Problem HS$_\mathbf{M}$. Find $2M + 3$ unknown real-valued functions $\{\mathbf{w}(s,t);\ \mathcal{G}(\mathbf{z};\zeta;t); \mathbf{z}_1(t), \ldots, \mathbf{z}_M(t)\}$, where $\mathbf{z}_k(t) = (z_{k,1}(t), z_{k,2}(t))$, $k = 1, \ldots, M$, and $\mathbf{w}(s,t) = (w_1(s,t), w_2(s,t)) : \partial\mathbb{U} \times I \to \mathbb{R}^2$ satisfying[2]
   (i) $\mathbf{w}(s,t) \in \Gamma(t)$ for all $(s,t) \in \partial\mathbb{U} \times I$;
   (ii) $\mathbf{w}(\cdot, t) : \partial\mathbb{U} \to \Gamma(t)$ is a $\mathcal{C}^2$-diffeomorphism for each fixed $t \in I$;
   (iii) $\mathbf{w}^{(0)}(s) = \mathbf{w}(s,0)$ is a given $\mathcal{C}^2$-diffeomorphism of the unit circle $\partial\mathbb{U}$,
which describes the boundary $\Gamma(0)$ of initial domain $\Omega_M(0)$;

---

[1] It is worth noting that the constants c, b_k, $d_{k,l}$ and q_k aren't dependent on any individual ε_k.

[2] Unknown magnitudes $\mathbf{w}$, $\mathcal{G}$, $\mathbf{z}_0$ depend on time t from a right-sided neighborhood I of $t = 0$. In fact, for our problem we need to determine the value of $\mathcal{G}(\mathbf{z};\zeta;t)$ only at the point $\zeta = O$, but we keep the extra variable ζ for computational reasons.

(iv) $\mathcal{G}(\mathbf{z};\zeta;t)$ is Green's function of the operator $-\triangle$ subject to the mixed boundary value problem, i.e. for each fixed $t \in I$

$$\Delta\mathcal{G}(\mathbf{z};\zeta;t) + \delta(\mathbf{z} - \zeta) = 0, \ \mathbf{z}, \zeta \in \Omega_M(t);$$

$$\mathcal{G}(\mathbf{z};\zeta;t) = 0, \ z \in \Gamma(t), \zeta \in \Omega_M(t);$$

$$\frac{\partial\mathcal{G}(\mathbf{z};\zeta;t)}{\partial n_{\mathbf{z}}} = 0, \ z \in \partial F_k(t), \zeta \in \Omega_N(t), k = 1, \dots, M;$$

(v) $\partial_t \mathbf{w}(s,t) = -\frac{Qh^2}{12\mu} \cdot \nabla\mathcal{G}(\mathbf{w}(s,t); O; t)$ for all $(s,t) \in \partial\mathbb{U} \times I$;

(vi) $\frac{d^2\mathbf{z}_k(t)}{dt^2} + \frac{\kappa_k\pi\varepsilon_k^2}{m_k}\frac{d\mathbf{z}_k(t)}{dt} =$

$$= \frac{Q\varepsilon_k}{m_k} \int\limits_0^{2\pi} \mathcal{G}(z_{k,1}(t)+\varepsilon_k\cos\theta, z_{k,2}(t)+\varepsilon_k\sin\theta; \zeta; t)\cdot\mathbf{n}^{(k)}(\theta)d\theta;$$

(vii) $\mathbf{z}_k(0) = \mathbf{z}_k^{(0)}$, $\mathbf{z}_k'(0) = \mathbf{z}_k^{(1)}$.

Here h is the width of the Hele-Shaw cell, μ is viscosity coefficient of fluid in the cell, Q is the strength of the source/sink, κ_k are the friction coefficients for the contact of k-th obstacle and the plates of the cell, $m_k = \pi\varepsilon_k^2\rho_k$ is the mass of the k-th obstacle, $\mathbf{n}^{(k)}(\theta)$ is the internal normal vector on the boundary of k-th obstacle, $k = 1, \dots, M$.

The function $\mathbf{w}(s,t) = (w_1(s,t), w_2(s,t))$ determines the parametrization of the unknown free boundary $\partial\Omega(t)$. Meanwhile the movement of each obstacle can be described in terms of the location of its variable center $\mathbf{z}_k(t)$, which is permissible as the inclusions are moving as rotation free rigid bodies. The assumption of non-rotation is valid as the small size and circular shape of each particle mean that the pressure function around its boundary can be assumed constant, while the term for friction with the fluid will be negligible compared to that between the particle and the plates of the cell. It is worth noting that the lubricative force between particles is not modeled in this paper, as it is not required to test the accuracy and limitations of the proposed system, however this can be added at a later time without requiring modification of the underlying analytical formulation.

Existence of the solution to the above problem can be shown in a way similar to that for existence of the solution for the flow in the Hele-Shaw cell with air bubbles in the flow (see, e.g. [21] and references therein).

The aim of our study is to get an approximate solution to the problem $\mathbf{HS_M}$, and to create a numerical system based upon it which describes the different behaviour of small obstacles in the Hele-Shaw flow.

3 Uniform representation of Green's function

The method of uniform asymptotic approximation of the Green's function related to different boundary value problems for a number of differential operators in singularly and regularly perturbed domains was created and developed by V. Maz'ya, A. Movchan and M. Nieves and is summarized in the recent book [3]. This method has additionally been used successfully to examine the

effect of an individual obstacle or particle in the Hele-Shaw cell [1,2]. In our analysis of **Problem HS$_\mathbf{M}$** slight modifications to the asymptotic formula for N_ε [19, (7.1)] are required, however as the method remains similar it won't be repeated here in full. The full details of the formulation and method are explained more fully in the supplementary material.

Let $\mathcal{G}_\varepsilon(\mathbf{x}, \mathbf{y})$ be Green's function of the Laplace operator $-\Delta$ with the zero Neumann data on $\partial F_k, k = 1, \ldots, M$, and the zero Dirichlet data on Γ. The function $\mathcal{G}_\varepsilon(\mathbf{x}, \mathbf{y})$ has the following asymptotic representation

$$\mathcal{G}_\varepsilon(\mathbf{x}, \mathbf{y}) = G^\Omega(\mathbf{x}, \mathbf{y}) + \sum_{k=1}^M \left\{ \mathcal{N}^{(k)}\left(\frac{\mathbf{x} - \mathbf{z}_k}{\varepsilon_k}, \frac{\mathbf{y} - \mathbf{z}_k}{\varepsilon_k}\right) + \frac{1}{2\pi}\log\left|\frac{\mathbf{x} - \mathbf{y}}{\varepsilon_k}\right| \right\} + \quad (3)$$

$$+ \sum_{k=1}^M \varepsilon_k \left\{ \mathcal{D}^{(k)}\left(\frac{\mathbf{x} - \mathbf{z}_k}{\varepsilon_k}\right) \cdot \nabla_\mathbf{x} H(\mathbf{z}_k, \mathbf{y}) + \mathcal{D}^{(k)}\left(\frac{\mathbf{y} - \mathbf{z}_k}{\varepsilon_k}\right) \cdot \nabla_\mathbf{y} H(\mathbf{x}, \mathbf{z}_k) \right\} + \mathbf{r}_\varepsilon(\mathbf{x}, \mathbf{y}),$$

where

$$|\mathbf{r}_\varepsilon(\mathbf{x}, \mathbf{y})| \le Const \cdot \varepsilon^2.$$

Here $\mathcal{N}^{(k)}$ are solutions to the modified Neumann problems in the exterior of $cl\,\omega_\varepsilon^{(k)}$, $\mathcal{D}^{(k)}$ are dipole vectors corresponding to inclusion $\omega_\varepsilon^{(k)}$ and H corresponds to the regular part of the Green's function.

The uniform estimate for the remainder in the above mentioned [19, Thm 7.1] is proved in L_∞-norm. It remains valid in our case for any multiply connected domain $\Omega_M(t)$ with sufficiently small interval I of time variable t.

In our case we accept the following notation for each instant of time $t \in I$.[3] $G^\Omega(\mathbf{x}, \mathbf{y}) = G(\mathbf{x}, \mathbf{y}; t)$ is Green's function of the Laplace operator $-\Delta$ for the simply connected domain $\Omega = \Omega(t)$ with zero Dirichlet data on $\partial\Omega(t)$, which is identical to that generating the representation presented in the case of one obstacle in [1], [2].

$$G^\Omega(\mathbf{x}; \mathbf{y}) := G(\mathbf{x}; \mathbf{y}; t) = -\frac{1}{2\pi}\log|g(\mathbf{x}, \mathbf{y})| \qquad (4)$$

This is the Green's function for the interior simply connected domain $\Omega(t)$. Here $g(\mathbf{x}, \mathbf{y}) = (g_1(\mathbf{y}, \mathbf{y}), g_2(\mathbf{x}, \mathbf{y})) : \Omega(t) \to \mathbb{U}$ is the normalized conformal mapping of $\Omega(t)$ onto the unit disc $\mathbb{U}$ ($g(\mathbf{x}, \mathbf{y})\big|_{\mathbf{x}=\mathbf{y}} = 0$, and $g'(\mathbf{x}, \mathbf{y})\big|_{\mathbf{x}=\mathbf{y}} > 0$). In our case $\mathbf{y} = \mathbf{O}$. If $g_0(\mathbf{x}) : \Omega(t) \to \mathbb{U}$ is any (non-normalized) mapping, then

$$g(\mathbf{x}, \mathbf{y}) = e^{-\arg g_0'(\mathbf{y})}\frac{g_0(\mathbf{x}) - g_0(\mathbf{y})}{1 - \overline{g_0(\mathbf{y})}g_0(\mathbf{x})}.$$

---

[3] Note, that in the case of one obstacle, this modified formula coincides with Maz'ya-Movchan-Nieves formula [3, (2.72)], cf. also [2].

In order to more easily express the final Neumann and Dirichlet functions we introduce auxiliary variables related to scaling of small obstacles

$$\xi_k = \frac{1}{\varepsilon_k}\left(\mathbf{x} - \mathbf{z}_k\right), \quad \eta_k = \frac{1}{\varepsilon_k}\left(\mathbf{y} - \mathbf{z}_k\right), \quad k = 1, \dots, M. \tag{5}$$

In these notations $\mathcal{N}^{(k)}(\xi_k, \eta_k)$, $k = 1, \dots, M$, are the Neumann functions for the exterior of the re-scaled obstacles F_k: The Neumann functions $\mathcal{N}^{(k)}(\xi_k, \eta_k)$, $k = 1, \dots, M$ possess in our case explicit representations (see, e.g., [22, p. 68]):

$$\mathcal{N}^{(k)}(\xi_k, \eta_k) = -\frac{1}{4\pi}\log|\xi_k - \eta_k|^2 - \tag{6}$$

$$-\frac{1}{4\pi}\log\left[\frac{(|\xi_k|^2 - 1)(|\eta_k|^2 - 1) + |\xi_k - \eta_k|^2}{|\xi_k|^2|\eta_k|^2}\right].$$

Meanwhile the Dirichlet functions, expressed for circular obstacles, are calculated from integrals using formula [23, (4.397.6)]:

$$\mathcal{D}_1^{(k)}(\xi_k) = \frac{1}{2}\frac{\xi_{k,1}}{(\xi_{k,1})^2 + (\xi_{k,2})^2}, \; \mathcal{D}_2^{(k)}(\xi_k) = \frac{1}{2}\frac{\xi_{k,2}}{(\xi_{k,1})^2 + (\xi_{k,2})^2}, \; k = 1, \dots, M. \tag{7}$$

In addition to the formulae for these functions solving **Problem HS$_\mathbf{M}$** requires both the derivatives and integrals to be calculated. These calculations are again placed in the appendix, and the results are expressed in Sect. 4.1.

4 Computational algorithm

With the asymptotic relationships required now derived, it is possible to articulate the approximate solution to **Problem HS$_\mathbf{M}$** and create a numerical model capable of performing simulations for multiple particles within the Hele-Shaw cell. Additionally, the results of these simulations can be used to more carefully examine the effect of initial particle distribution on both the evolution of the fluid boundary and the dynamic behaviour of the particles themselves.

4.1 Final system of differential equations

It follows from the potential theory (see, e.g. [13, Ch. 8], cf. [19, Lemma 5.1]), that for any compact subset D, $\overline{D} \subset \Omega_N(t)$

$$\left(r_\varepsilon(\mathbf{x}, \mathbf{y})\right)'_{x_j} \leq \varepsilon^3, \; j = 1, 2, \; \mathbf{x}, \mathbf{y} \in \overline{D}.$$

Thus, the Problem (**HS$_\mathbf{M}$**) can be asymptotically approximated by the following system of equations

$$\partial_t w_j(\mathbf{w}; \mathbf{0}; \mathbf{z}) = -\frac{Qh^2}{12\mu}\left(\partial_{x_j} G(\mathbf{w}; \mathbf{O}) + \Upsilon_j(\mathbf{w}; \mathbf{0}; \mathbf{z})\right) \tag{8}$$

$$\frac{d^2 z_{k,j}}{dt^2} + \frac{\kappa \pi \varepsilon_k^2}{m_k} \frac{dz_{k,j}(t)}{dt} = \frac{Q \varepsilon_k^2}{m_k} I_j^{(k)} - c \, \text{sign}\left(\frac{dz_{k,j}(t)}{dt}\right) \left|\frac{dz_{k,j}(t)}{dt}\right|^2, \quad k = 1, \dots, M, \tag{9}$$

where:

$$\Upsilon_j = \sum_{k=1}^{M} \left(K_j^{(k)} + \partial_{w_j} J_1^{(k)}(\mathbf{w}; \mathbf{O}) + \partial_{w_j} J_2^{(k)}(\mathbf{w}; \mathbf{O}) \right), \quad j = 1, 2 \tag{10}$$

with initial conditions $\mathbf{z}_k(0) = \mathbf{z}_k^{(0)}$, $\mathbf{z}_k'(0) = \mathbf{z}_k^{(1)}$. Here $\mathbf{w} = (w_1(s,t), w_2(s,t))$ is an unknown parametrization of the external boundary $\partial D(t)$, $\mathbf{z}_k = (z_{k,1}(t), z_{k,2}(t))$ are unknown position of the center of the moving obstacles. The additional term in the right side of (9) represents the drag force, where c is a constant computed as: $c = 0.5 h c_x \varepsilon_k \rho / m_k$, and c_x stands for the drag coefficient, while ρ denotes the fluid density.

Here, in the right hand-side of equations (8), (10) we use formulas derived more fully in the supplementary material, namely

$$\partial_{x_j} G^{\Omega}(w_1(s,t), w_2(s,t); 0, 0) = \tag{11}$$

$$= -\frac{1}{2\pi} \left(g_1(w_1(s,t), w_2(s,t); 0, 0) \partial_{w_j} g_1(w_1(s,t), w_2(s,t); 0, 0) + \right.$$

$$\left. + g_2(w_1(s,t), w_2(s,t); 0, 0) \partial_{w_j} g_2(w_1(s,t), w_2(s,t); 0, 0) \right).$$

$$K_j^{(k)} = -\frac{1}{2\pi} \left\{ \frac{(w_j - z_{k,j})(z_{k,1}^2 + z_{k,2}^2) + \varepsilon_k^2 z_{k,j}}{[(w_1 - z_{k,1})^2 + (w_2 - z_{k,2})^2 - \varepsilon_k^2][z_{k,1}^2 + z_{k,2}^2 - \varepsilon_k^2] + \varepsilon_k^2(w_1^2 + w_2^2)} - \right. \tag{12}$$

$$\left. - \frac{w_j - z_{k,j}}{(w_1 - z_{k,1})^2 + (w_2 - z_{k,2})^2} \right\}.$$

$$\partial_{x_1} J_1^{(k)}(\mathbf{w}, O) = \frac{\varepsilon_k^2}{2} \left(\frac{(w_2 - z_{k,2})^2 - (w_1 - z_{k,1})^2}{((w_1 - z_{k,1})^2 + (w_2 - z_{k,2})^2)^2} \cdot \partial_{x_1} H(\mathbf{z}_k; O) - \right. \tag{13}$$

$$\left. - \frac{2(w_1 - z_{k,1})(w_2 - z_{k,2})}{((w_1 - z_{k,1})^2 + (w_2 - z_{k,2})^2)^2} \cdot \partial_{x_2} H(\mathbf{z}_k; O) \right),$$

and

$$\partial_{x_2} J_1^{(k)}(\mathbf{w}, O) = \frac{\varepsilon_k^2}{2} \left(-\frac{2(w_1 - z_{k,1})(w_2 - z_{k,2})}{((w_1 - z_{k,1})^2 + (w_2 - z_{k,2})^2)^2} \cdot \partial_{x_1} H(\mathbf{z}_k; O) - \right. \tag{14}$$

$$\left. - \frac{(w_2 - z_{k,2})^2 - (w_1 - z_{k,1})^2}{((w_1 - z_{k,1})^2 + (w_2 - z_{k,2})^2)^2} \cdot \partial_{x_2} H(\mathbf{z}_k; O) \right),$$

where the derivatives $\partial_{x_j} H(\mathbf{z}_k; \mathbf{O})$ are:.

$$\partial_{x_j} H(\mathbf{z}_k; O) = \frac{1}{2\pi} \frac{g_1(\mathbf{z}_k; O) \partial_{z_{k,j}} g_1(\mathbf{z}_k; O) + g_2(\mathbf{z}_k; O) \partial_{z_{k,j}} g_2(\mathbf{z}_k; O)}{g_1^2(\mathbf{z}_k; O) + g_2^2(\mathbf{z}_k; O)} - \tag{15}$$

$$- \frac{1}{2\pi} \frac{z_{k,j}}{z_{k,1}^2 + z_{k,2}^2}.$$

At last

$$\partial_{x_j} J_2^{(k)}(\mathbf{w}, O) = \frac{\varepsilon_k^2}{2} \frac{z_{k,1}}{z_{k,1}^2 + z_{k,1}^2} \cdot \partial_{w_j} F_1(\mathbf{w}; \mathbf{z}_k) + \frac{\varepsilon_k^2}{2} \frac{z_{k,2}}{z_{k,1}^2 + z_{k,1}^2} \cdot \partial_{w_j} F_2(\mathbf{w}; \mathbf{z}_k).$$

(16)

where

$$F_j := \partial_{y_j} H(\mathbf{w}; \mathbf{z}_k) = \frac{1}{2\pi} \frac{g_1(\mathbf{w}; \mathbf{z}_k)\partial_{z_{k,j}} g_1(\mathbf{w}; \mathbf{z}_k) + g_2(\mathbf{w}; \mathbf{z}_k)\partial_{z_{k,j}} g_2(\mathbf{w}; \mathbf{z}_k)}{g_1^2(\mathbf{w}; \mathbf{z}_k) + g_2^2(\mathbf{w}; \mathbf{z}_k)} +$$

(17)

$$+ \frac{1}{2\pi} \frac{w_j - z_{k,j}}{(w_1 - z_{k,1})^2 + (w_2 - z_{k,2})^2}, \ j = 1, 2, \ k = 1, \dots, M.$$

Finally, the right-hand side of remaining equations (9) is given by:

$$I_j^{(k)} = \frac{g_1(\mathbf{z}_k; \mathbf{O})\partial_{z_{k,j}} g_1(\mathbf{z}_k; \mathbf{O}) + g_2(\mathbf{z}_k; \mathbf{O})\partial_{z_{k,j}} g_2(\mathbf{z}_k; \mathbf{O})}{g_1^2(\mathbf{z}_k; \mathbf{O}) + g_2^2(\mathbf{z}_k; \mathbf{O})} + 3\frac{z_{k,j}}{z_{k,1}^2 + z_{k,2}^2}. \quad (18)$$

4.2 Description of the scheme

The computational scheme to solve the problem is analogical to that presented in [2]. It employs reduction of the system of governing equations (8)-(9) to the dynamic system of the first order. To this end an additional dependent variable, the velocity of particle, is introduced:

$$\mathbf{v}_k = \mathbf{z}_k'. \quad (19)$$

Thus, for the boundary curve discretized by N points and for the M inclusions inside the domain, one obtains a system composed of $2N + 4M$ ordinary differential equations. The system is solved by the standard MatLab ODE tool: ode45. The conformal mappings of the domain free boundary are performed by the Schwarz-Christoffel toolbox [24,25], with the derivatives of the mapping calculated using subroutines based on spline approximation. When the particles collisions are detected the computations are discontinued. New initial conditions are then defined assuming either; a perfectly elastic impact, or a purely inelastic impact (which is achieved by 'fusing' the original particles together into a single, perfectly circular, particle with a larger radius and preserving the objects mass). Next, the computational process is resumed with the new initial conditions.

In all simulations, as the asymptotic approximation reduces in accuracy near the source/sink, or near to the fluid boundary, three conditions are imposed to prevent the results being adversely affected. The first two conditions are that, for any particle k, there must always be a minimum distance of ε_k to the source/sink and to the fluid boundary. Additionally it will be required that the minimum radial distance between the source/sink and the fluid boundary always remains larger than 0.1.

5 Numerical examples and discussions

5.1 Computational accuracy

In order to investigate the accuracy of computations we use two analytical benchmarks. The first one is based on the classical solution by Polubarinova-Kochina [5, p. 29]. It describes evolution of the fluid front in the domain without inclusions ($\varepsilon = 0$) for both, the fluid sink and source. In [2] it was used to define the accuracy of computations for such a limiting case. Unfortunately there is no analytical solution for the problem with inclusions[4]. To circumvent this deficiency we shall modify the basic system of equations by supplementing relation (8) with an additional term:

$$\partial_t w_j(\mathbf{w}; \mathbf{0}; \mathbf{z}) = -\frac{Qh^2}{12\mu} \left(\partial_{x_j} G(\mathbf{w}; \mathbf{O}) + \Upsilon_j(\mathbf{w}; \mathbf{0}; \mathbf{z}) - \Upsilon_j(\tilde{\mathbf{w}}; \mathbf{0}; \mathbf{z}) \right), \qquad (20)$$

where $\tilde{\mathbf{w}}(s, t)$ is a solution by Polubarinova-Kochina. In this way, $\tilde{\mathbf{w}}(s, t)$ becomes a solution of the system: (20), (9). Modification (20) can be interpreted as the introduction of a special leak-off function (see [26]).

The second benchmark is built in exactly the same way on the assumption that the reference solution, $\tilde{\mathbf{w}}(s, t)$, describes a circular shape. Its evolution in time, defined by the radius $R(t)$, can be easily determined from the fluid balance.

Note that the aforementioned manner of benchmark construction can be applied for any known $\mathbf{w}(s, t)$ being a solution of the system:

$$\partial_t w_j(\mathbf{w}; \mathbf{0}; \mathbf{z}) = -\frac{Qh^2}{12\mu} \partial_{x_j} G(\mathbf{w}; \mathbf{O}). \qquad (21)$$

In Fig.2 we present the evolution of the fluid free boundary for both benchmark cases. For the fluid sink variant a transition from curve 1 to curve 2 is implemented (domain contraction), while for the fluid source a reverse direction of domain transformation takes place (domain expansion). The initial positions of inclusions are marked schematically by two types of circles: solid line for three inclusions, dashed line for eight inclusions. In our analysis we will consider both, the immobile (fixed at initial positions) and moving inclusions. For the fixed inclusions the governing system of equations reduces to (20), where in the right hand side the predefined values of $\mathbf{z}$ are introduced. The error of computations will be described by the relative error of radius vector $\rho(\theta, t)$ defining the fluid boundary.

In the first test we investigate the influence of the number and size of inclusions on the solution accuracy. To this end, the Polubarinova benchmark is considered. The boundary curve is discretized by $N = 140$ points. The

---

[4] An analytical solution in the case of a single circular inclusion is forthcoming (J.S. Marshall: Analytical solutions for Hele-Shaw moving boundary flows in the presence of a circular cylinder), but there are currently no published solutions for circular inclusions with which to compare.

computational errors at the final time, $\delta\rho(\theta, t_{max})$, are shown in Fig.3-Fig.4 for the fluid sink and source respectively, for the case of immobile inclusions. Three different values of ε (0.1, 0.01, 0.001) are used. For a reference we depict also the error distribution for the case of no inclusions. The preliminary conclusion from this test is that regardless of the number and sizes of inclusions slightly better accuracy is obtained for the domain expansion. This observation is in line with the trend reported in [2], where also a better stability of computations for the fluid source variant was noted. It shows that a general tendency of accuracy deterioration with growing ε is present. The results for $\varepsilon = 0.001$ are in fact of the same quality as those for $\varepsilon = 0$, but even for $\varepsilon = 0.01$ the error distribution indicates that its average value is very close to that for $\varepsilon = 0$. There is not much difference in accuracy for different number of inclusions, except for the case of $\varepsilon = 0.1$, where for the fluid sink one obtains distinctly worse results. However, even then the maximal solution error is still below one percent. Note that in such a case ε is no longer a small parameter.

For the second benchmark example, the circular domain, we obtained similar trends (for this reason we do not illustrate them), but the solution accuracy was slightly better.

In the next test we shall consider to what degree the inclusions movement affects the accuracy of computations. Let us analyze the Polubarinova benchmark in the fluid source configuration for eight inclusions. Again three values of ε are considered: 0.1, 0.01, 0.001. For each of these variants we compare the error of computations, $\delta\rho$, obtained for moving and immobile inclusions. The results of this comparison are depicted in Fig.5. It shows that the level of accuracy is the same for both, moving and immobile inclusions. Only some slight differences in error distribution can be observed. Again, the accuracy gradation depends on the size of inclusions, giving the substantial deterioration only for the biggest inclusion $\varepsilon = 0.1$.
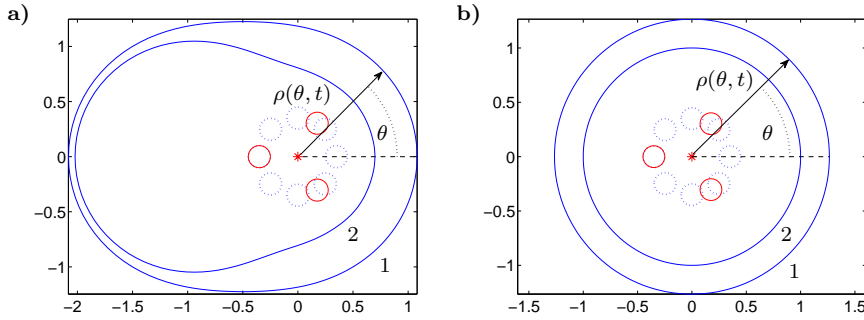

Fig. 2 Domain configuration for the benchmark examples: a) Polubarinova solution, b) circular domain. Fluid source/sink is located at the origin. Depending on the chosen variant, the domain expands from curve 2 to 1 or contracts from 1 to 2. Radius vector $\rho(\theta, t)$ defines the boundary shape. Two configuration of inclusions are shown: solid lines - three inclusions, dashed lines - eight inclusions.
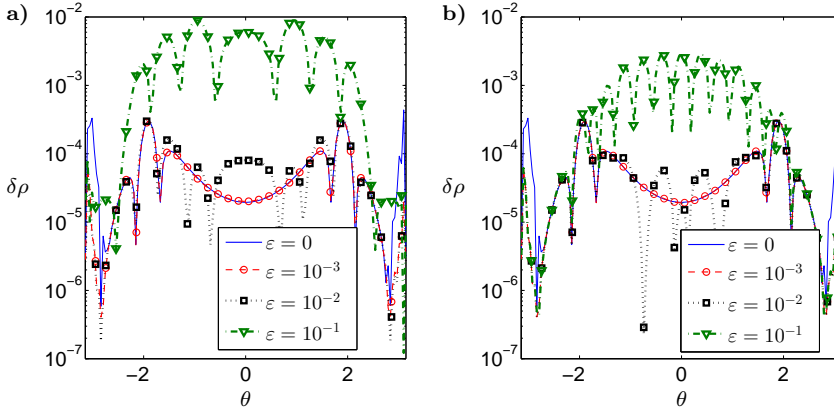
Fig. 3 The relative error of the radius vector $\rho(\theta, t_{max})$ for the Polubarinova benchmark for: a) three immobile inclusions, b) eight immobile inclusions. The fluid sink variant was analyzed. The boundary curve was discretized by N=140 points.
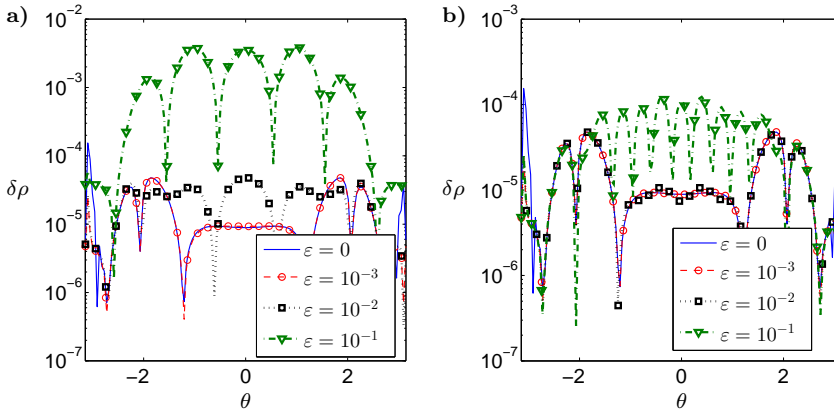

Fig. 4 The relative error of the radius vector $\rho(\theta, t_{max})$ for the Polubarinova benchmark for: a) three immobile inclusions, b) eight immobile inclusions. The fluid source variant was analyzed. The boundary curve was discretized by N=140 points.

In the last test we investigate to what degree the density of discretization of the fluid free boundary affects the accuracy of computations. This time both benchmarks, the Polubarinova and circular domain solutions, are in use. We consider the fluid sink variant for eight inclusions of different sizes ($\varepsilon = \{0.1, 0.01, 0.001\}$). A number of simulations was performed for N varying from 20 to 140. For every value of N, the maximal and average errors of the radius vector $\rho(\theta, t_{max})$ were computed. The results are depicted in Fig.6, where for comparison also the curves for $\varepsilon = 0$ are shown. Respective curves for the maximal error are distinguished by the circular markers, while triangular markers are used for the average errors. The make the graphs more legible, the
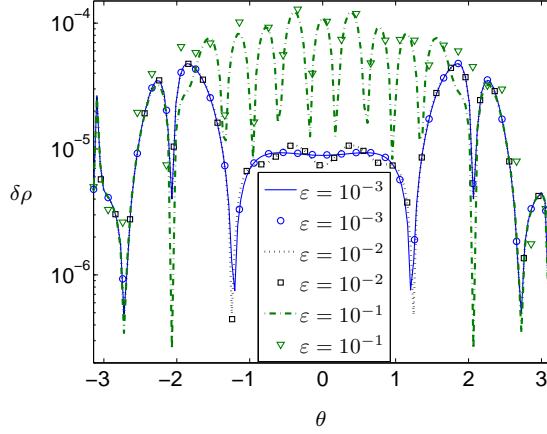
Fig. 5 The relative error of the radius vector $\rho(\theta, t_{max})$ for 8 fixed and moving inclusions of different sizes. The Polubarinova benchmark for the fluid source configuration was used. The boundary curve was discretized by $N = 140$ nodes. The results denoted by markers only refer to the moving inclusions.
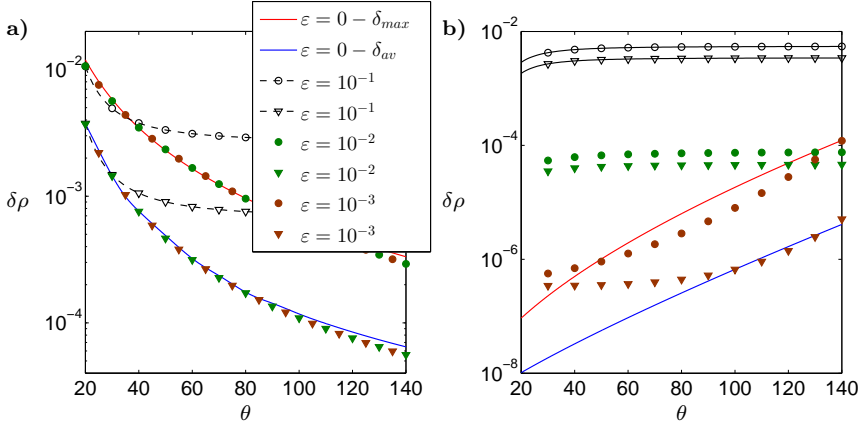

Fig. 6 The relative errors of the radius vector for the sink variant of the problem related to the number of the boundary nodes N: δ_{max} - the maximal error (circular markers), δ_{av} - the average error (triangular markers). Respective graphs refer to: a) the Polubarinova benchmark, b) the circular domain benchmark.

results for $\varepsilon = \{0.01, 0.001\}$ are denoted by markers only. For the Polubarinova benchmark there is a clear trend of accuracy increase with growing N. The results for $\varepsilon = \{0.01, 0.001\}$ are almost identical as those for no-inclusions case. Appreciable deterioration of accuracy is obtained for $\varepsilon = 0$, however even here the errors stabilize at the level 10^{-3}. Quite different situation is observed for the circular domain benchmark. Here, a counterintuitive tendency of error increase with growing number of boundary nodes is clear. It can be explain by

the fact that for a regular shape and the spline approximation of the derivatives along the boundary (which in the case of a circle is an accurate one) a small number of points is sufficient to produce very good results. An increase in N leads here to the cumulation of the computational errors. For this reason, such a trend is much less distinct for $\varepsilon = 0$, where it is the presence of very large inclusions which introduces the greatest errors. Note that the results for $\varepsilon = \{0, 0.001, 0.01\}$ obtained when taking $N = 140$ are of the same accuracy level as for the Polubarinova benchmark.

5.2 Collision strategies and particle interactions

In any fluid containing multiple particles and an explicit boundary there exist a multitude of forces which aren't directly accounted for within the present model. Rotational forces, such as the Saffman and Magnus forces, needn't be considered here as the model assumes that the particles are non-rotating. Further effects such as the virtual mass and Basset forces on particle movement are likely to be small compared to the friction term from their contact with the cell wall (see [27] for more information on related forces).

The primary situation in which forces arise for which additional algorithms are required is the case of particle collision. In principle use of the Green's function should prevent particle overlap, however as an asymptotic approximation is used this possibility isn't eliminated within the final system of equations directly. Complicating matters further is the fact that, for particle collisions within a fluid, the lubricative force prevents both perfectly elastic and inelastic collisions, and it also decelerates particles near to the boundary (see [28]). Determining the exact effect of this force on the final dynamics of the system however is beyond the scope of this paper.

To compensate for this two separate steps are taken. The first is to increase the friction coefficient of particles which become close to the boundary, which can be easily achieved and prevents any objects leaving the fluid domain. The second is that, in the case of particle collisions, both the perfectly elastic and inelastic cases will be modeled. While this will not produce the most accurate representation of the dynamics of particle interaction within the fluid these two cases provide the opposing ends of the spectrum, and as such if both can be modeled then the more accurate case involving the lubricative force can added later through the use of additional algorithms. Further these cases are very computationally efficient, and will ensure the model does not become overly cumbersome.

Simulations in the case of two particles with various properties, obtained for both elastic and inelastic collisions, are shown in Fig. 8, while the setup is displayed in Fig. 7. The post-collision particle movement is determined from the conservation of momentum combined with; conservation of energy in the
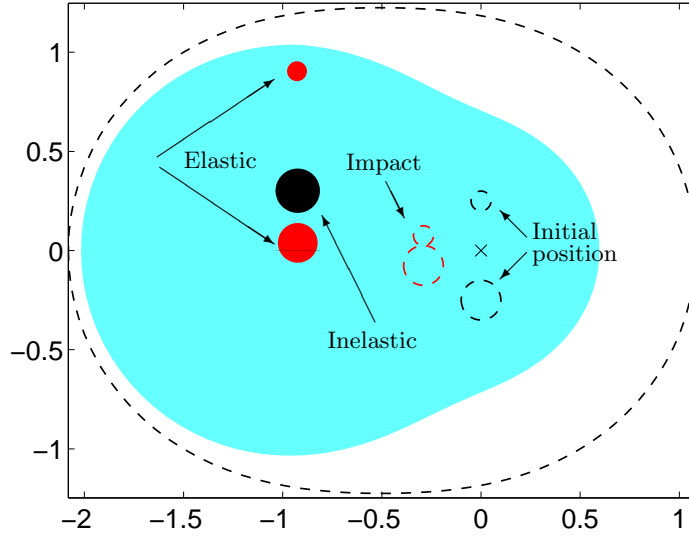
Fig. 7 Diagram simulation for elastic and inelastic impacts. Here the black dotted lines show the initial positions, the red dotted line indicates the moment of particle collision, the red and blue coloured areas provide the final particle and fluid positions respectively, and the marker 'x' indicates the position of the fluid sink.
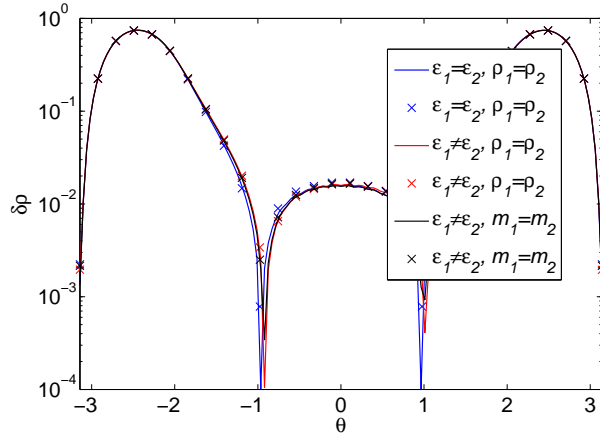

Fig. 8 The deviation of the final boundary, relative to the case without inclusions, when two particles collide. Here the lines indicate elastic collisions, while markers indicate inelastic collisions. The particles properties are defined by their radius, ε, density, ρ and mass m.

elastic case, and the conservation of mass and volume for inelastic events. The

initial fluid boundary is taken from the solution to the first order Polubarinova-Kochina system in the case of a sink, with the final time taken as $t = 0.7$. Here $Qh^2/24\pi\mu = 1$, $\rho = 2.8$, $\kappa = 0.01$ and initially $\varepsilon = \{0.1, 0.05\}$.

In the conducted tests, the presence of a small number of particle collisions lead to only a minimal increase in the computation time, and the decrease in accuracy was negligible compared to that induced by other parameters. Additionally it is clear from results concerning the relative boundary deformation between cases (Fig. 8) that the difference between perfectly elastic and inelastic collisions is relatively small compared with the total change in boundary deformation. The fact that the collision type has only a minor influence on the deformation of the free boundary only improves the case for these efficient approximations over the more intensive option of computing the lubricative force.

5.3 Particle position and parameters

With the abilities of the model established, we can now use it to examine the effect of particle inclusion on the fluid flow within the Hele-Shaw cell. The flow can be best understood as traveling in the shortest possible straight line to the boundary (sink) from the source (boundary). Particles placed in the path of this line will redirect the flow around it. Therefore positioning objects near to the source/sink will disrupt the largest portion of the domain, as the proportion of the flow disturbed is greatest, and the fluid on the opposite side of the source/sink will extend/drain faster to compensate. Conversely obstacles near the boundary will produce very localized effects, although these effects will be far larger in magnitude.

As a result of the fluid flow behaving in this manner the shape of the domain, size of the inclusions and movement of the particles over time will play a crucial role in determining the effect of particle placement on the fluid boundary evolution. Particles with a low (or zero) initial velocity, or a sufficiently high friction coefficient, will remain almost stationary relative to the movement of the fluid. In such situations the large magnitude localized effects are often only present over short time periods. Similarly a small inclusion size will only disrupt a small portion of the fluid flow, and as such the overall effects will be minimal.

These differing effects on the boundary can be displayed using simple system in which a variety of particles are placed within an initial domain defined by the Polubarinova solution. Note that differing configurations of particles will be utilized. A diagram showing the setup is provided in Fig. 9, while the relative deviation of the boundary from the case without inclusions is provided in Fig. 10. It is worth stating that, in the case with M particles, inclusions $k = 1, .., M$ will be taken. Additionally the particles are given an initial veloc-

ity of zero, as this will best demonstrate the effects on the boundary in absence of additional factors, with the remaining material parameters kept identical to those used in the previous subsection.

The localized effects for particles near the boundary, and wider domain effects for particles near the source, are both clearly present in Fig. 10a. Additionally it can be seen in Fig. 10b that these effects compound as the number of particles increases. These results perfectly match the previous description in terms of the fluid flowing between the source and the boundary. Further the results are well within the expected level of accuracy for this problem variant (see Fig. 4, $\varepsilon = 10^{-1}$).

5.4 Simulations with many particles

While there is no theoretical maximum for the number of particles which can be simulated the computation time will obviously become a limiting factor. In practice the particle numbers which can be reasonably computed is far more dependent on the distance between each particle and; adjacent particles, the source/sink and the boundary. As a result, with proper initial distribution, simulations involving hundreds of particles can be easily completed within a reasonable computation time (typically $1.5 - 4.5$ hours).
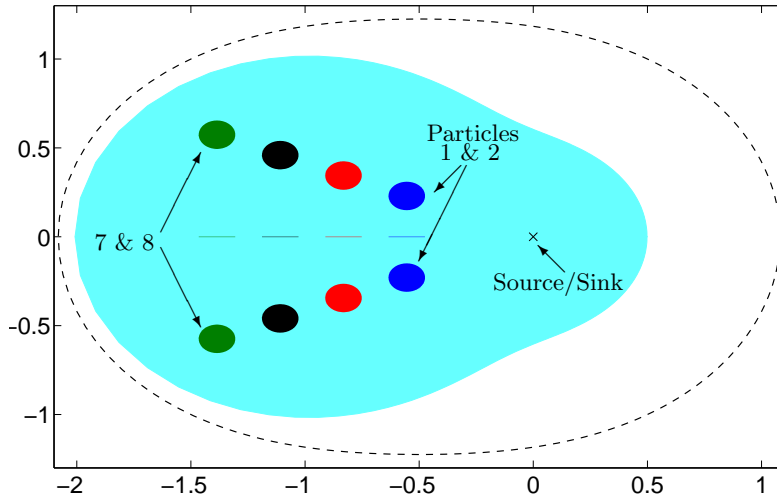

Fig. 9 Diagram simulation for initially stationary particles in a 'Line' formation. Here the black dotted line shows the final boundary position, the light blue coloured area provides the initial fluid position and the marker 'x' indicates the position of the fluid source. The coloured circles indicate the initial particle positions, with particles: (1,2) heavy blue, (3,4) red, (5,6) black and (7,8) green.
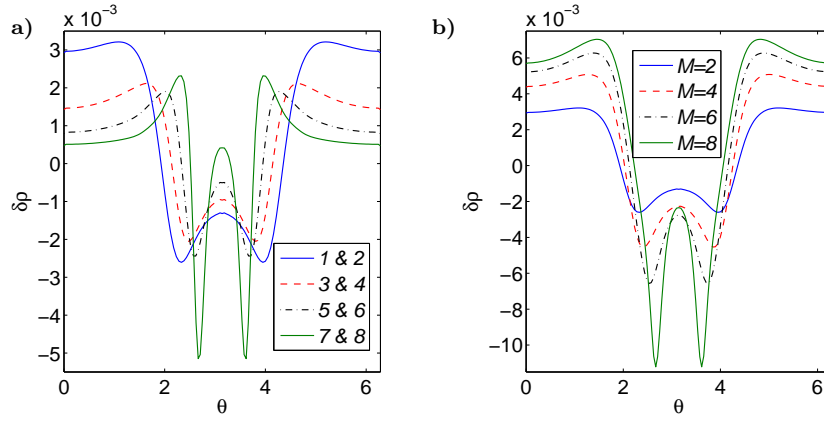
Fig. 10 Comparison of the relative radial distance to the fluid boundary, $\delta\rho$, measured at the final time, when there are (a) two particles (b) M particles within the fluid at different radial distances to the boundary in the case of a fluid source.

Four demonstrative examples are considered, with systems containing either 120 or 540 particles in an ordered or semi-random distribution. The ordered system was defined by distributing particles into 8 rings around the source, within a fluid domain defined by a unit circle. Semi-random distributions where meanwhile created by splitting the initial domain into separate rings, and choosing particle angles and radial positions within each ring using MatLab's random number function, rejecting particle positions which lead to overlaps. The initial volume fraction of particles within the fluid was kept constant between cases, such that $\varepsilon = 10^{-2}$ for 540 particles. A diagram showing the initial distributions is shown in Fig. 11, while the resulting boundary deformation over a time period of $t = 0.1$ is shown in Fig. 12.

It is clear from Fig. 12 that the deformation of the boundary in the case with many particles is far more complicated than those previously examined, with systems containing particles with a similar distribution and identical volume fractions resulting in notably different changes to the fluid boundary. That the systems with particles in an ordered distribution had a more periodic and predictable effect on the boundary deformation is not surprising, however the fact that simulations involving large numbers of particles lead to a far smoother boundary deformation in both cases, and can easily be conducted using this model, provides a method by which internal effects can be more readily studied.

6 Outline and discussion

An asymptotic approximation of the fluid flow within a Hele-Shaw cell containing multiple free-moving particles has been been obtained, which models
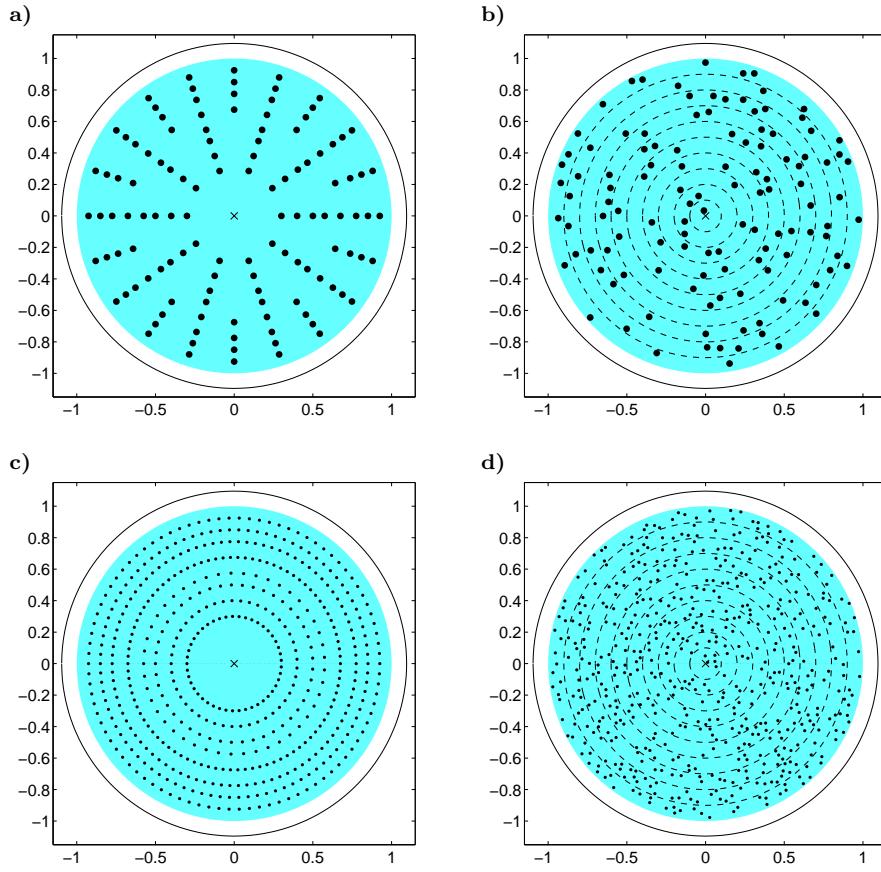
Fig. 11 Diagram showing the initial position of the boundary (blue fill), the initial distribution of the (a,b) $M = 120$ (c,d) $M = 540$ particles, and the expected final boundary position is denoted by a black dashed line. Here the particle distributions are (a,c) ordered or (b,d) generated semi-randomly.

both the movement of the fluid boundary and the inclusions. A model based on this system of equations has been created in a MatLab environment, which is capable of dealing with situations involving hundreds of particles and any potential collisions between them. The accuracy of the final model was assessed for various numbers and sizes of inclusions.

A brief examination into the effect of the particle inclusion on the fluid flow, primarily through the resulting boundary distortion, was conducted. The key finding was the dual nature of the effect of initial particle distribution on the fluid boundary, with particles close to the boundary causing very localized effects, while those near to the source/sink affect the wider domain.
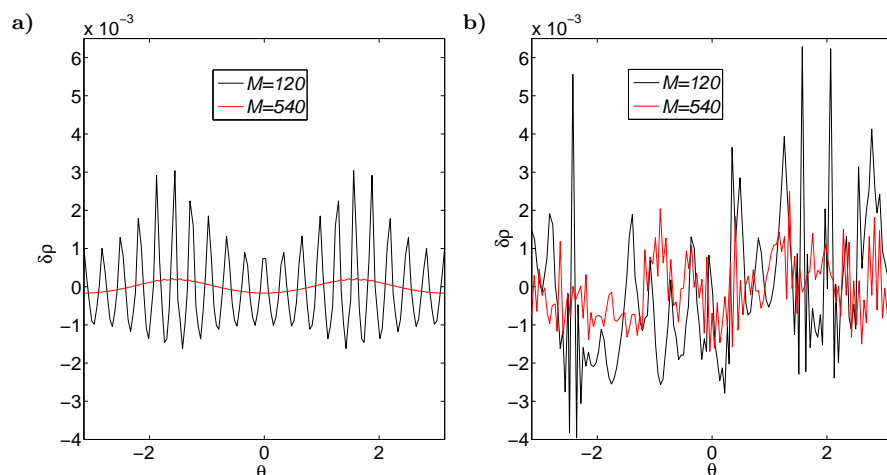
Fig. 12 The relative deformation of the boundary between the cases with $M = 120, 540$ particles and the case without inclusions. Here (a) is for particles in an ordered distribution, while (b) is for a semi-random distribution.

We now have a credible tool with which to simulate the fluid flow in a narrow channel subject to the presence of multiple different inclusions and obstacles. This has clear applicability, namely with regards to investigating the effective properties of the fluid when it contains a large number of particles.

References

1. G. Mishuris, S. Rogosin, M.Wrobel, Hele-Shaw Flow with a small obstacle, *Meccanica*, **49**, 2014, 2037–2047.
2. G. Mishuris, S. Rogosin, M.Wrobel, Moving Stone in the Hele-Shaw Flow *LMS J. Mathematika*, **61** (2), 2015, 457-474.
3. V. Maz'ya, A. Movchan, M. Nieves, *Green's Kernel and Meso-Scale Approximations in Perforated Domains*. Lecture Notes in Mathematics, **2077**, Springer, Heidelberg etc., 2013.
4. H. S. Hele-Shaw, The flow of water, *Nature.* **58(1489)**, 1898, 33–36.
5. B. Gustafsson, A. Vasil'ev, *Conformal and Potential Analysis in Hele-Shaw cells*, Birkhäuser Verlag, Basel-Boston-Berlin, 2006.
6. A. M. Meirmanov, *The Stefan Problem*. W. de Gruyter, Berlin - New York, 1992.
7. S. Richardson, Hele Shaw flows with a free boundary produced by the injection of fluid into a narrow channel, *J. Fluid Mech*, **56**, No. 4, 1972, 609-618.
8. P. Abbyad, R. Dangla, A. Alexandrou, C.N. Baroud, Rails and anchors: guiding and trapping droplet microreactors in two dimensions, *Lab on a Chip*, **11**, 2011, 813-821.

9. A. M. Meirmanov, I. V. Nekrasova, Mathematical models to hydraulic shock in slighty viscous fluid, *Math. Model. Comp. Simul.* **4**, No. 6, 2012, 597–610.

10. G. Mishuris, M.Wrobel, A. Linkov, On modeling hidraulic fracture in proper variables: stiffness, accuracy, sensitivity, *Int. J. Eng. Sci.* **61**, 2012, 10–23.

11. Yu.E. Hohlov, M. Reissig, On classical solvability for the Hele-Shaw moving boundary problem with kinetic undercooling regularization, *Euro. J. Applied Math.*, **6**, 1995, 421–439.

12. G.B. Folland, *Introduction to Partial Differential Equations*, 2nd ed., Princeton Univ. Press, Princeton, N.J., 1995.

13. D. Gilbarg, N.S. Trudinger, *Elliptic Partial Differential Equations of Second Order*, Springer, Berlin etc., 1983.

14. A.D. Polyanin, *Handbook of Linear Partial Differential Equations for Engineers and Scientists*, Chapman&Hall/CRC Press, Boca Raton - London, 2002.

15. A.D. Polyanin, V.F. Zaitsev, *Handbook of Nonlinear Partial Differential Equations*, 2nd ed., CRC Press, Boca Raton - London - New York, 2012.

16. J. Hadamard, Sur le problème d'ánalyse relatif à équilibre des plaques elastiques encastrees. *Memoire couronne en 1907 par lÁcademie: Prix Vaillant, Mémoires présentés par divers savants à lÁcademie des Sciences*, **33**, No. 4, 1908. In *Oeuvres de Jasques Hadamard*, vol. **2** (Centre National de la Recherche Scientifique, Paris, 1968), 515–629.

17. V. Maz'ya, A. Movchan, Uniform asymptotics of Green's kernels for mixed and Neumann problems in domains with small holes and inclusions. Isakov, Victor (ed.), *Sobolev spaces in mathematics. III: Applications in mathematical physics.* New York, NY: Springer; Novosibirsk: Tamara Rozhkovskaya Publisher. International Mathematical Series **10**, 2009, 277–316.

18. V. Maz'ya, A. Movchan, Uniform asymptotics of Green's kernels in perforated domains and meso-scale approximation, *Complex Variables and Elliptic Equations*, **57**, No. 2, 2012. 137–154.

19. V. Maz'ya, A. Movchan, M. Nieves, Green's kernels for transmission problems in bodies with small inclusions. In: *Operator Theory and Its Applications. In Memory of V.B. Lidskii (1924–2008)* (M. Levitin, D. Vassiliev Eds.), AMS, Providence, Rhode Island, 2010, 127–160.

20. S.N. Antontsev, C.R. Gonçalves, A.M. Meirmanov, Exact estimate for the classical solutions to the free-boundary problem in the Hele-Shaw cell, *Adv. Diff. Equ.* **8**, No. 10, 2003, 1259–1280.

21. V. Entov, P. Etingof, On the break of air bubbles in a Hele-Shaw cell, *Eur. J. Appl. Math.*, **22**, No. 2, 2011, 125-149.

22. N. Papamichael, *Lectures on Numerical Conformal Mapping*, University of Cyprus, 2008.

23. I. S. Gradshteyn, I. M. Ryzhik, *Table of Integrals, Series, and Products*, Academic Press, Amsterdam-Boston etc., 2007 (7th edition).

24. T. A. Driscoll, Algorithm 756: A MATLAB Toolbox for Schwarz-Christoffel mapping, *ACM Trans. Math. Soft.*, **22**, 1996, 168–186.

25. T. A. Driscoll, Algorithm 843: Improvements to the Schwarz–Christoffel toolbox for MATLAB. *ACM Trans. Math. Soft.*, **31**, 2005, 239–251.

26. M. Wrobel, G. Mishuris, Hydraulic fracture revisited: Particle velocity based simulation. International Journal of Engineering Science, **94**, 2015, 23-58.

27. H.P. Zhu, Z.Y. Zhou, R.Y. Yang, A.B. Yu, Discrete particle simulation of particulate systems: Theoretical developments, *Chemical Engineering Science*, **62**, 2007, 3378–3396.

28. A. Lavrov, H. Laux, DEM modeling of particle restitution coefficient vs Stokes number: The role of lubrication force. In: *6th International Conference on Multiphase Flow (ICMF 2007)*, Leipzig, Germany, July 9-13, 2007, paper S2_Thu_C_54.